

Investigation and Analysis of Mismatching Properties for Nanoscale Strained MOSFETs

Jack Jyun-Yan Kuo, *Student Member, IEEE*, William Po-Nien Chen, and Pin Su, *Member, IEEE*

Abstract—This paper investigates and analyzes the matching properties of nanoscale strained MOSFETs under various bias conditions. Through a comprehensive comparison between coprocessed strained and unstrained PMOSFETs, the impact of process-induced uniaxial strain on the matching performance of MOS devices has been assessed and analyzed. Our examination indicates that, in the low-gate-voltage-overdrive ($|V_{gst}|$) regime, the normalized drain current mismatch ($\sigma(\Delta I_d)/I_d$) of the strained device is almost the same as that of the unstrained one at a given transconductance to drain current ratio (g_m/I_d). In the high $|V_{gst}|$ linear regime, the $\sigma(\Delta I_d)/I_d$ for the strained device is smaller than that of the unstrained one because of its smaller normalized current factor mismatch. In the high $|V_{gst}|$ saturation regime, the improvement in the $\sigma(\Delta I_d)/I_d$ for the strained device is further enhanced because of the reduced critical electric field at which the carrier velocity becomes saturated.

Index Terms—Fluctuation, mismatch, transconductance to drain current ratio, uniaxial strained silicon, variation.

I. INTRODUCTION

WITH the scaling of device dimensions [1], [2], the device mismatching that stems from stochastic fluctuations is becoming a concern for nanoscale MOSFETs [1]–[4]. Device mismatch may limit the achievable accuracy in analog applications such as multiplexed analog systems, digital-to-analog converters, reference source, and the synchronous RAM (SRAM), etc. [1]–[4]. Since strained silicon is widely used in state-of-the-art CMOS technologies to enable the mobility scaling [1], [7]–[15], a comprehensive study regarding the impact of strain on device mismatch is needed. Through a comparison between strained and unstrained devices, this study investigates and analyzes the mismatching properties of nanoscale strained MOSFETs.

This paper is organized as follows. Section II introduces the devices and measurement used in this study. In Sections III and IV, we examine the impact of strain on the matching performance for devices biased in the low-gate-voltage-overdrive regime and high-gate-voltage-overdrive regime, respectively. Section V draws the conclusion.

Manuscript received August 8, 2008; revised May 18, 2009. First published June 16, 2009; current version published March 10, 2010. The review of this paper was arranged by Associate Editor T. Hiramoto. This work was supported in part by the National Science Council of Taiwan under Contract NSC98-2221-E-009-178, and in part by the Ministry of Education in Taiwan under ATU Program.

The authors are with the Department of Electronics Engineering and Institute of Electronics, National Chiao Tung University, Hsinchu 30050, Taiwan (e-mail: jack.ee93g@nctu.edu.tw; williamchen.ee93g@nctu.edu.tw; pinsu@faculty.nctu.edu.tw).

Color versions of one or more of the figures in this paper are available online at <http://ieeexplore.ieee.org>.

Digital Object Identifier 10.1109/TNANO.2009.2025596

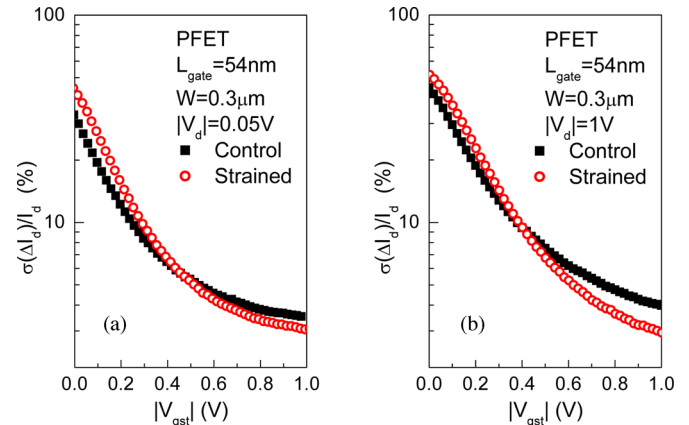


Fig. 1. Comparison of $\sigma(\Delta I_d)/I_d$ versus $|V_{gst}|$ for strained and unstrained devices at (a) $|V_d| = 0.05$ V, and (b) $|V_d| = 1$ V, respectively.

II. DEVICES AND MEASUREMENT

The devices used in this study were fabricated by state-of-the-art process-induced uniaxial strained-silicon technology. Coprocessed strained and unstrained PMOSFETs were investigated [16] (with channel direction $\langle 110 \rangle$ on (100) silicon substrate). The strained device features compressive uniaxial contact etch stop layer (CESL) and SiGe source/drain. For the transistors with gate length $L_{gate} = 54$ nm, the saturated drain current (I_{dsat}) of the strained device is improved more than 100% as compared with its control counterpart [16].

The mismatching properties of strained and unstrained devices were measured from identical devices in a matching pair configuration on 60 dies. Statistics on the mismatch in drain current (ΔI_d), threshold voltage, and current factor ($\Delta\beta$) in the linear and saturation regions were analyzed. The threshold voltage (V_{th}) was measured by the constant-current method and β was determined by the maximum slope method [17].

III. MATCHING PERFORMANCE IN THE LOW $|V_{gst}|$ REGIME

Fig. 1(a) and (b) shows the V_g dependence of the extracted standard deviations of normalized drain current mismatch ($\sigma(\Delta I_d)/I_d$) for strained and control devices with $L_{gate} = 54$ nm and gate width (W) = $0.3 \mu\text{m}$ in the linear region ($|V_d| = 0.05$ V) and saturation region ($|V_d| = 1$ V), respectively. It can be seen that, for gate voltage overdrive ($|V_{gst}| = |V_g| - |V_{th}|$) below 0.4 V, the $\sigma(\Delta I_d)/I_d$ of the strained device is larger than that of the unstrained one. On the other hand, for $|V_{gst}|$ above 0.4 V, the $\sigma(\Delta I_d)/I_d$ of the strained device is smaller than that of the unstrained one.

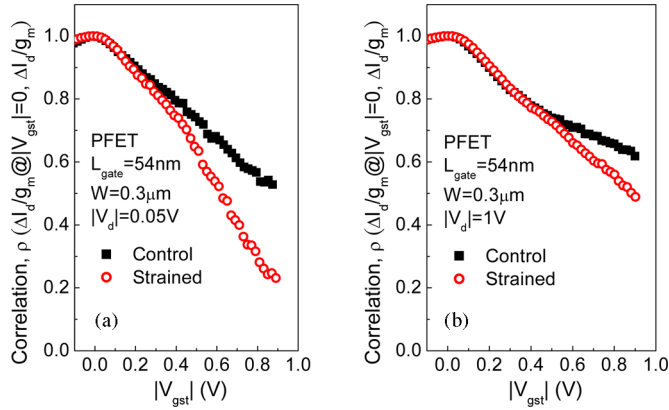


Fig. 2. Correlation between $(\Delta I_d)/g_m$ at $|V_{gst}| = 0$ and $(\Delta I_d)/g_m$ at other $|V_{gst}|$ at (a) $|V_d| = 0.05$ V, and (b) $|V_d| = 1$ V, respectively.

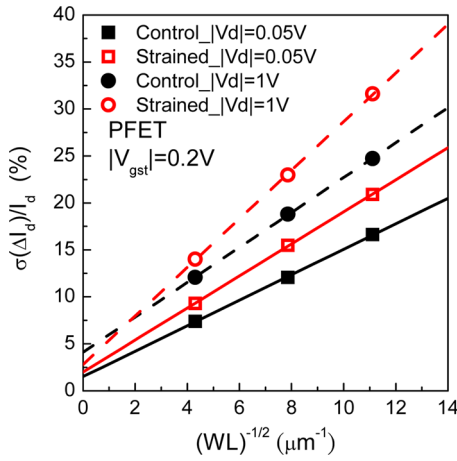


Fig. 3. Pelgrom plot of $\sigma(\Delta I_d)/I_d$ showing larger $(\Delta I_d)/I_d$ for the strained device at $|V_{gst}| = 0.2$ V with $|V_d| = 0.05$ and 1 V.

The normalized drain current mismatch in the low $|V_{gst}|$ regime (e.g., $|V_{gst}| < 0.4$ V) is dominated by the threshold voltage mismatch [17], and can be expressed as [18]

$$\frac{\Delta I_d}{I_d} = -\frac{g_m}{I_d} \times (\Delta V_{th}) \quad (1)$$

where g_m is the transconductance. To verify the relevance of ΔV_{th} to $\Delta I_d/I_d$ [17], (1) can be rewritten as $(\Delta I_d)/g_m = -\Delta V_{th}$ and the correlation (ρ) between $(\Delta I_d)/g_m$ at $|V_{gst}| = 0$ and $(\Delta I_d)/g_m$ at other $|V_{gst}|$ is shown in Fig. 2. It can be seen from Fig. 2 that the correlation lies between 70% and 100% for both strained and control devices for $|V_{gst}| < 0.4$ V. This ensures that the threshold voltage mismatch is the dominant mechanism that determines the normalized drain current mismatch in the low $|V_{gst}|$ linear regime.

Fig. 3 shows the Pelgrom plot of $\sigma(\Delta I_d)/I_d$ at $|V_{gst}| = 0.2$ V. The geometries of the devices in Fig. 3 are $W/L_{gate} = 1 \mu\text{m}/54 \text{ nm}$, $0.3 \mu\text{m}/54 \text{ nm}$, and $0.12 \mu\text{m}/54 \text{ nm}$. Note that the L_{gate} of the strained device needs to be the same in order to keep similar strain in the channel. This is because the channel strain is gate-length dependent in process-induced strain silicon

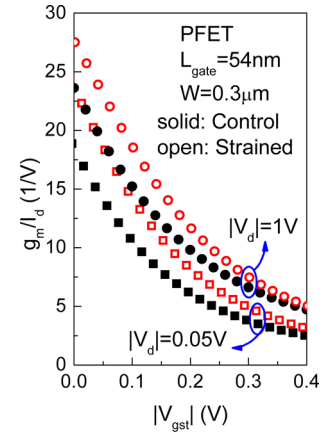


Fig. 4. g_m/I_d for the strained device is enhanced in the low $|V_{gst}|$ regime at $|V_d| = 0.05$ and 1 V.

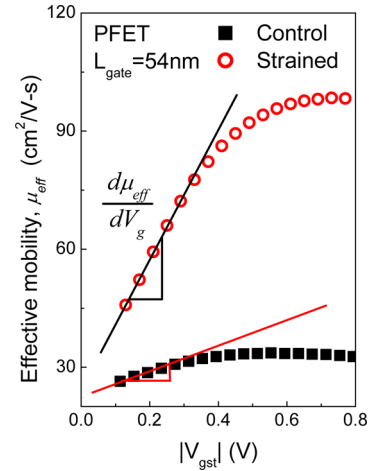


Fig. 5. Extracted carrier mobility versus $|V_{gst}|$ showing that the strained device has larger V_g sensitivity in the low $|V_{gst}|$ regime.

devices [10]–[13]. From Fig. 3, it can be seen that $\sigma(\Delta I_d)/I_d$ of the strained device is larger than that of the control device.

Fig. 4 shows that the g_m/I_d of the strained device is significantly larger than the control device. It is the enhanced g_m/I_d that increases the drain current mismatch in the low $|V_{gst}|$ regime [see (1)]. The g_m/I_d in the linear region and saturation region can be modeled by (2) and (3), respectively, derived from Berkeley Short-channel IGFET Model (BSIM) [19]:

$$\frac{g_m}{I_d} = \frac{1}{V_{gst} - V_d/2} + \frac{\partial \mu_{eff}/\partial V_g}{\mu_{eff}} \quad (2)$$

$$\frac{g_m}{I_d} = \frac{1}{V_{gst}} \left[\frac{V_{gst} + 2E_{sat}L_{eff}}{V_{gst} + E_{sat}L_{eff}} \right] + \frac{E_{sat}L_{eff}}{V_{gst} + E_{sat}L_{eff}} \frac{\partial \mu_{eff}/\partial V_g}{\mu_{eff}} \quad (3)$$

where L_{eff} and E_{sat} denote the effective channel length and the critical electric field at which the carrier velocity becomes saturated, respectively. The g_m/I_d for the strained device is higher than its control counterpart because of the higher V_g sensitivity of carrier mobility (μ_{eff}) present in the strained device, as shown in Fig. 5. It can be seen from Fig. 5 that μ_{eff} increases with V_g in

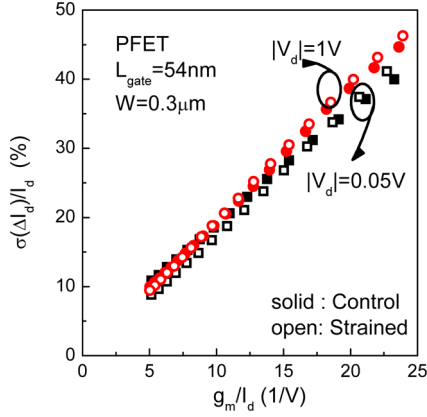


Fig. 6. $\sigma(\Delta I_d)/I_d$ versus g_m/I_d for strained and unstrained devices.

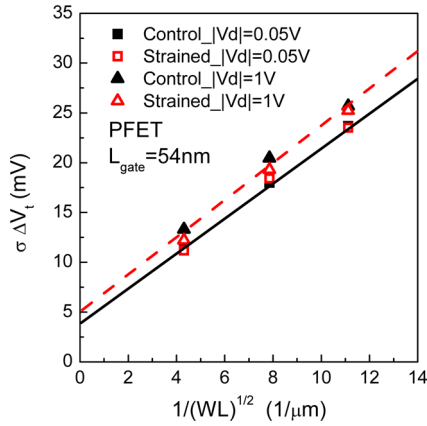


Fig. 7. Pelgrom plot of ΔV_{th} showing nearly identical ΔV_{th} for the strained and unstrained devices.

the low $|V_{gst}|$ regime. This is because in the low $|V_{gst}|$ regime, the mobility is mainly determined by Coulombic scattering [20]. The mobile carrier screening makes μ_{eff} increases with V_g . The larger slope of the mobility for the strained device is responsible for the higher g_m/I_d , as observed in Fig. 4.

Nevertheless, for a given g_m/I_d , the $\sigma(\Delta I_d)/I_d$ for the strained and control devices are nearly identical, as shown in Fig. 6. In other words, the V_{th} mismatch for the strained and control devices are nearly the same, as demonstrated in Fig. 7. Note that a linear dependence of $\sigma(\Delta V_{th})$ on $1/(WL_{gate})^{-1/2}$ in the Pelgrom plot indicates a random-dopant-fluctuations origin of V_{th} mismatch [21]. Moreover, the increase of $\sigma(\Delta V_{th})$ with increasing $|V_d|$ due to drain-induced barrier lowering (DIBL) can also be observed in Fig. 7 [22].

IV. MATCHING PERFORMANCE IN THE HIGH $|V_{gst}|$ REGIME

In the high $|V_{gst}|$ regime (e.g., $|V_{gst}| > 0.4$ V), Fig. 1(a) and (b) shows smaller $\sigma(\Delta I_d)/I_d$ for the strained device as compared with the unstrained one. The Pelgrom plot of $\sigma(\Delta I_d)/I_d$ at $|V_{gst}| = 0.8$ V in Fig. 8 also shows a smaller $\sigma(\Delta I_d)/I_d$ for the strained device. Furthermore, the correlation between $(\Delta I_d)/g_m$ at $V_{gst} = 0$ and $(\Delta I_d)/g_m$ at other V_{gst} shown in Fig. 2 implies that ΔV_{th} is not the only dominant mechanism

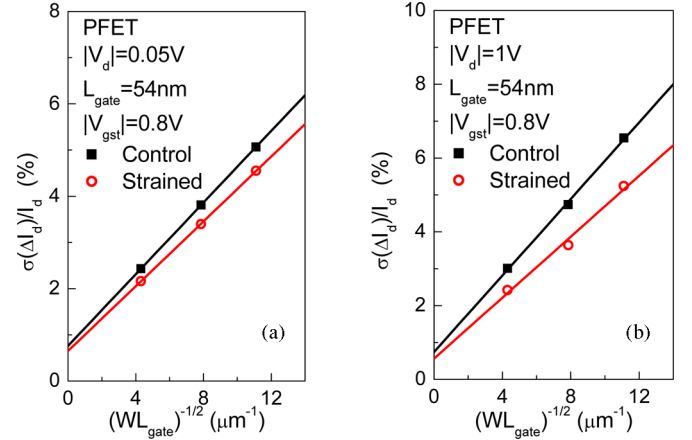


Fig. 8. Pelgrom plot of $\sigma(\Delta I_d)/I_d$ shows smaller $(\Delta I_d)/I_d$ for the strained device at $|V_{gst}| = 0.8$ V with (a) $|V_d| = 0.05$ V, and (b) $|V_d| = 1$ V, respectively.

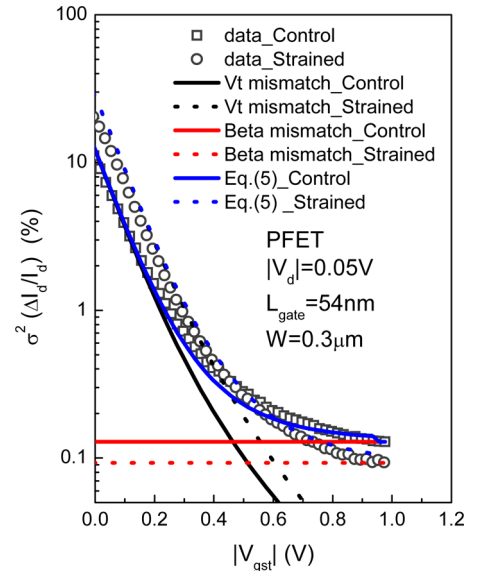


Fig. 9. $\sigma^2(\Delta I_d)/I_d$ can be modeled well by (5).

in the high $|V_{gst}|$ regime. In other words, the current factor mismatch ($\Delta\beta$) should be included in the following normalized drain current mismatch expression as [6]:

$$\frac{\Delta I_d}{I_d} = -\frac{g_m}{I_d} \times (\Delta V_{th}) + \frac{\Delta\beta}{\beta}. \quad (4)$$

The variance of the normalized drain current mismatch is [23], [24]:

$$\sigma^2\left(\frac{\Delta I_d}{I_d}\right) = \left(\frac{g_m}{I_d}\right)^2 \times \sigma^2(\Delta V_{th}) + \sigma^2\left(\frac{\Delta\beta}{\beta}\right). \quad (5)$$

A. Linear Region

Fig. 9 shows a comparison of the measured $\sigma^2(\Delta I_d)/I_d$ with (5) at $|V_d| = 0.05$ V. It can be seen that the $\sigma^2(\Delta I_d)/I_d$ can be modeled well by considering the contribution from both ΔV_{th} and $\Delta\beta$. Moreover, Fig. 9 indicates that the normalized linear

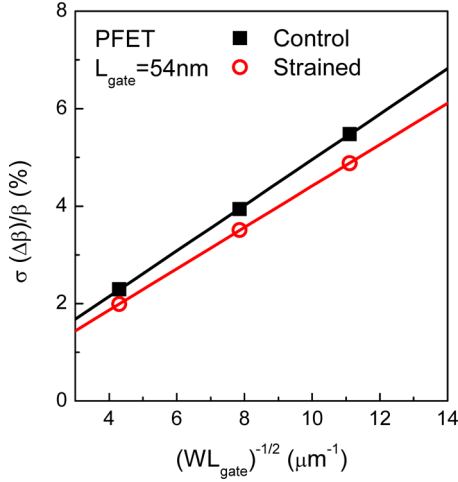


Fig. 10. Pelgrom plot of $\sigma(\Delta I_d)/I_d$ showing smaller $\sigma(\Delta\beta)/\beta$ for the strained device.

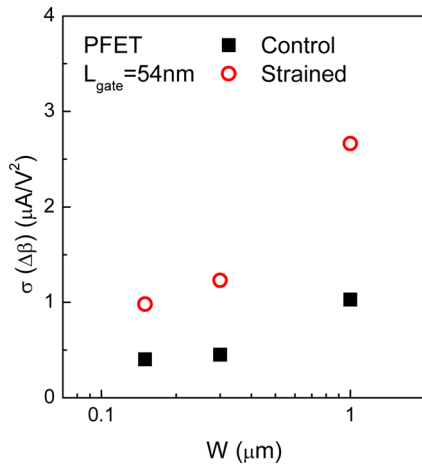


Fig. 11. $\sigma(\Delta\beta)$ versus gate width showing larger $\sigma(\Delta\beta)$ for the strained device.

drain current mismatch in the high $|V_{gst}|$ regime is dominated by $\Delta\beta/\beta$.

The smaller $\sigma(\Delta\beta)/\beta$ for the strained device shown in Fig. 10 further demonstrates that it is the reduced $\sigma(\Delta\beta)/\beta$ that reduces the linear drain current mismatch in the high $|V_{gst}|$ regime. It should be noted that although the $\sigma(\Delta\beta)/\beta$ of the strained device is smaller than that of the unstrained one, the $\sigma(\Delta\beta)$ is actually larger for the strained device, as shown in Fig. 11. This implies that the improvement of $\sigma(\Delta\beta)/\beta$ for the strained device results from the increased β . The increased β can be attributed to the strain-enhanced carrier mobility.

In order to further understand the enhanced $\sigma(\Delta\beta)$ in the strained device, we have performed low-frequency noise measurements. This is because carrier mobility fluctuations show their presence in the low-frequency noise characteristics. Through a careful extraction, we found that the Hooge parameter, which represents the degree of mobility fluctuations [25], is significantly larger for the strained device as compared with the unstrained one (see Fig. 12). It is plausible that the increased $\sigma(\Delta\beta)$ results from the strain enhanced mobility fluctuation.

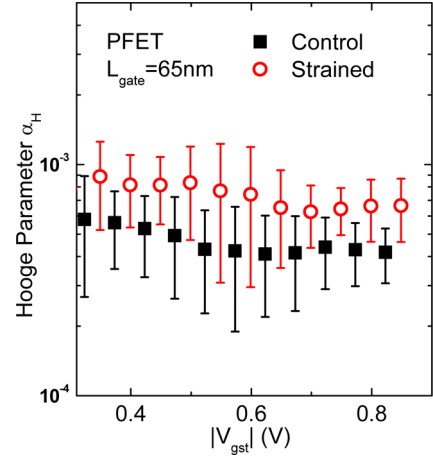


Fig. 12. Hooge parameter versus $|V_{gst}|$ showing larger degree of mobility fluctuations for the strained device.

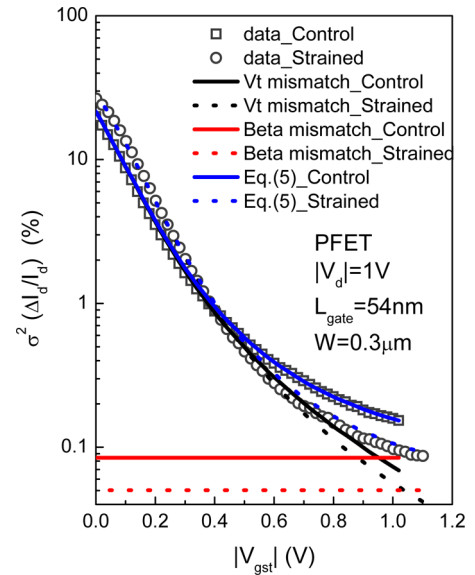


Fig. 13. $\sigma^2(\Delta I_d)/I_d$ in saturation region ($|V_d| = 1$ V) showing the importance of the V_{th} mismatch in the high $|V_{gst}|$ (e.g., $|V_{gst}| = 0.8$ V) regime.

B. Saturation Region

As compared with Fig. 8(a), Fig. 8(b) shows larger discrepancies in $\sigma(\Delta I_d)/I_d$ between strained and unstrained devices. In other words, the improvement in $\sigma(\Delta I_d)/I_d$ for the strained device is further enhanced in saturation region. Both Figs. 2(b) and 13 indicate that the V_{th} mismatch is still relevant to the overall $\sigma(\Delta I_d)/I_d$ in the high $|V_{gst}|$ saturation region. In other words, the excess improvement of $\sigma(\Delta I_d)/I_d$ for the strained device in saturation region results from the reduced V_{th} mismatch. The reduced V_{th} mismatch can be explained by the strain-reduced g_m/I_d in the high $|V_{gst}|$ saturation region (e.g., $|V_d| = 1$ V), as shown in Fig. 14.

The reduced g_m/I_d in the high $|V_{gst}|$ saturation region for the strained device can be attributed to the strain-reduced E_{sat} [26] [see the first term in (3)]. The strain-reduced E_{sat} results from the enhanced carrier mobility in the strained device. The

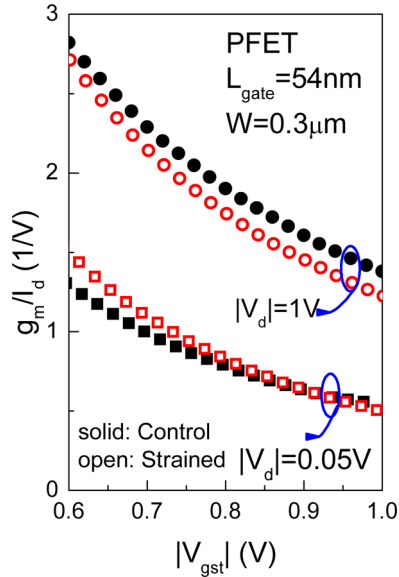


Fig. 14. The g_m/I_d for the strained device in the high $|V_{gst}|$ saturation regime ($|V_d| = 1$ V) is smaller than the control counterpart.

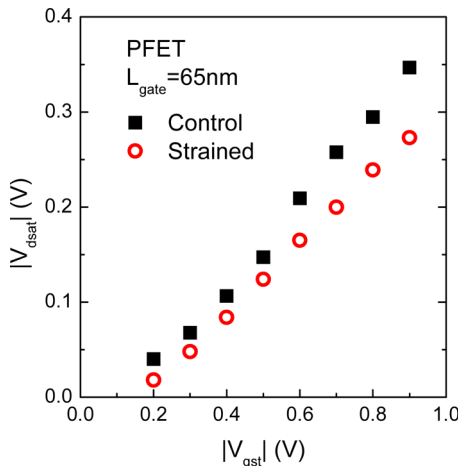


Fig. 15. $|V_{dsat}|$ versus $|V_{gst}|$ indicating a smaller E_{sat} for the strained device.

enhancement in carrier mobility corresponds to an increase in slope of the carrier velocity versus lateral field characteristic and a reduction in the critical field (E_{sat}) for velocity saturation [26]. The strain-reduced E_{sat} can be verified by the extracted drain saturation voltage (V_{dsat}) [26], which is essentially determined by E_{sat} in the high $|V_{gst}|$ regime [27]. The extracted V_{dsat} shown in Fig. 15 implies a smaller E_{sat} for the strained device. It is the reduced E_{sat} that results in a smaller g_m/I_d , and thus, further enhances the $\sigma(\Delta I_d)/I_d$ improvement for the strained device in the high $|V_{gst}|$ saturation region shown in Fig. 8(b).

V. CONCLUSION

We have investigated and analyzed the mismatching properties of nanoscale strained PMOSFETs under various bias conditions. In the low $|V_{gst}|$ regime, the $\sigma(\Delta I_d)/I_d$ for the strained device is enhanced while the threshold voltage mismatch of the strained device is nearly identical to that of the control one. The

increased $\sigma(\Delta I_d)/I_d$ for the strained device can be attributed to the enhanced g_m/I_d . In other words, the $\sigma(\Delta I_d)/I_d$ of the strained device is almost the same as the unstrained one at a given g_m/I_d . In the high $|V_{gst}|$ linear region, the smaller $\sigma(\Delta I_d)/I_d$ for the strained device results from its smaller $\sigma(\Delta\beta)/\beta$, albeit the $\sigma(\Delta\beta)$ for the strained device is larger than that of the unstrained one. In the high $|V_{gst}|$ saturation regime, the improvement in $\sigma(\Delta I_d)/I_d$ for the strained device is further enhanced because of the strain-reduced E_{sat} .

REFERENCES

- [1] C. Hu, "Device challenges and opportunities," in *VLSI Symp. Tech. Dig.*, 2004, pp. 4–5.
- [2] F. Boeuf, M. Sellier, A. Farcy, and T. Skotnicki, "An evaluation of the CMOS technology roadmap from the point of view of variability, interconnects, and power dissipation," *IEEE Trans. Electron. Devices*, vol. 55, no. 6, pp. 1433–1440, Jun. 2008.
- [3] A. Bhavnagarwala, S. Kosonocky, C. Radens, K. Stawiasz, R. Mann, Q. Ye, and K. Chin, "Fluctuation limits & scaling opportunities for CMOS SRAM cells," in *IEDM Tech. Dig.*, Dec. 2005, pp. 675–678.
- [4] S. Saxena, C. Hess, H. Karbasi, A. Rossoni, S. Tonello, P. McNamara, S. Lucherini, S. Minehane, C. Dolainsky, and M. Quarantelli, "Variation in transistor performance and leakage in nanometer-scale technologies," *IEEE Trans. Electron. Devices*, vol. 55, no. 1, pp. 131–144, Jan. 2008.
- [5] M. Vergret, "The analog challenge of nanometer CMOS," in *IEDM Tech. Dig.*, 2006, pp. 1–8.
- [6] M. J. M. Pelgrom, A. C. J. Duinmaijer, and A. P. G. Welbers, "Matching properties of MOS transistors," *IEEE J. Solid-State Circuits*, vol. 24, no. 5, pp. 1433–1439, May 1989.
- [7] H. Ohta, N. Tamura, H. Fukutome, M. Tajima, K. Okabe, A. Hatada, K. Ikeda, K. Ohkoshi, T. Mori, K. Sukegawa, S. Satoh, and T. Sugii, "High performance sub-40 nm bulk CMOS with dopant confinement layer (DCL) technique as a strain booster," in *IEDM Tech. Dig.*, 2007, pp. 1–4.
- [8] Y. Tateshita, J. Wang, K. Nagano, T. Hirano, Y. Miyamoto, T. Ikuta, T. Kataoka, Y. Kikuchi, S. Yamaguchi, T. Ando, K. Tai, R. Matsumoto, S. Fujita, C. Yamane, R. Yamamoto, S. Kanda, K. Kugimiya, T. Kimura, T. Ohchi, Y. Yamamoto, Y. Nagahama, Y. Hagimoto, H. Wakabayashi, Y. Tagawa, M. Tsukamoto, H. Iwamoto, M. Saito, S. Kadomura, and N. Nagashima, "High-performance and low-power CMOS device technologies featuring metal/high-k gate stacks with uniaxial strained silicon channels on (100) and (110) substrates," in *IEDM Tech. Dig.*, 2006, pp. 1–4.
- [9] S. Tyagi, C. Auth, P. Bai, G. Curello, H. Deshpande, S. Gannavaram, O. Golonzka, R. Heussner, R. James, C. Kenyon, S.-H. Lee, N. Lindert, M. Liu, R. Nagisetty, S. Natarajan, C. Parker, J. Sebastian, B. Sell, S. Sivakumar, A. St Amour, and K. Tone, "An advanced low power, high performance, strained channel 65 nm technology," in *IEDM Tech. Dig.*, 2005, pp. 245–248.
- [10] S. E. Thompson, M. Armstrong, C. Auth, M. Alavi, M. Buehler, R. Chau, S. Cea, T. Ghani, G. Glass, T. Hoffman, C.-H. Jan, C. Kenyon, J. Klaus, K. Kuhn, M. Zhiyong, B. McIntyre, K. Mistry, A. Murthy, B. Obradovic, R. Nagisetty, N. Phi, S. Sivakumar, R. Shaheed, L. Shifren, B. Tufts, S. Tyagi, M. Bohr, and Y. El-Mansy, "A 90-nm logic technology featuring strained-Si," *IEEE Trans. Electron. Devices*, vol. 51, pp. 1790–1797, Nov. 2004.
- [11] S. E. Thompson, G. Sun, K. Wu, J. Lim, and T. Nishida, "Key differences for process-induced uniaxial vs. substrate-induced biaxial stressed Si and Ge channel MOSFETs," in *IEDM Tech. Dig.*, 2004, pp. 221–227.
- [12] S. E. Thompson, G. Sun, Y. S. Choi, and T. Nishida, "Uniaxial-process-induced strained-Si: extending the CMOS roadmap," *IEEE Trans. Electron. Devices*, vol. 53, no. 5, pp. 1010–1020, May 2006.
- [13] X. Chen, S. Fang, W. Gao, T. Dyer, Y. W. Teh, S. S. Tan, Y. Ko, C. Baiocco, A. Ajmera, J. Park, J. Kim, R. Stierstorfer, D. Chidambarrao, Z. Luo, N. Nivo, P. Nguyen, J. Yuan, S. Panda, O. Kwon, N. Edleman, T. Tjoa, J. Widodo, M. Belyansky, M. Sherony, R. Amos, H. Ng, M. Hierlemann, D. Coolbough, A. Steegen, I. Yang, J. Sudijono, T. Schiml, J. H. Ku, and C. Davis, "Stress proximity technique for performance improvement with dual stress linear at 45 nm Technology and beyond," in *VLSI Symp. Tech. Dig.*, 2006, pp. 8.1.1–8.1.2.
- [14] M. Shima, K. Okabe, A. Yamaguchi, T. Sakoda, K. Kawamura, S. Watanabe, T. Isome, K. Okoshi, T. Mori, Y. Hayami, H. Minakata, A. Hatada,

- Y. Shimamune, A. Katakami, H. Ota, T. Sakuma, T. Miyashita, K. Hosaka, H. Fukutome, N. Tamura, T. Aoyama, K. Sukegawa, M. Nakaishi, S. Fukuyama, S. Nakai, M. Kojima, S. Sato, M. Miyajima, K. Hashimoto, and T. Sugii, "High-performance low operation power transistor for 45 nm node universal applications," in *VLSI Symp. Tech. Dig.*, 2006, pp. 19.3.1–19.3.2.
- [15] D. V. Singh, K. A. Jenkins, J. Sleight, Z. Ren, M. Jeong, and W. Haensch, "Strained ultrahigh performance fully depleted nMOSFETs with ft of 330 GHz and sub-30-nm gate lengths," *IEEE Electron. Device Lett.*, vol. 27, no. 3, pp. 191–193, Mar. 2006.
- [16] J. J.-Y. Kuo, W. Chen, and P. Su, "A comprehensive investigation of analog performance for uniaxial strained PMOSFETs," *IEEE Trans. Electron. Devices*, vol. 56, no. 2, pp. 284–290, Feb. 2009.
- [17] J. A. Croon, M. Rosmeulen, S. Decoutere, W. Sansen, and H. E. Maes, "An easy-to-use mismatch model for the MOS transistor," *IEEE J. Solid-State Circuits*, vol. 37, no. 8, pp. 1056–1064, Aug. 2002.
- [18] E. A. Vittoz, "The design of high-performance analog circuits on digital CMOS chips," *IEEE J. Solid-State Circuits*, vol. SC-20, no. 3, pp. 657–665, Mar. 1985.
- [19] Y. Cheng and C. Hu, *MOSFET Modeling & BSIM3 User's Guide*, ON, Canada: KAP, 1999.
- [20] W. Chen, P. Su, and K. Goto, "Investigation of Coulomb mobility in nanoscale strained PMOSFETs," *IEEE Trans. Nanotechnol.*, vol. 7, no. 5, pp. 538–543, Sep. 2008.
- [21] M. Miyamura, T. Fukai, T. Ikezawa, R. Ueno, K. Takeuchi, and M. Hane, "SRAM critical field evaluation based on comprehensive physical/statistical modeling considering anomalous non-Gaussian intrinsic transistor fluctuations," in *VLSI Symp. Tech. Dig.*, 2007, pp. 22–23.
- [22] O. Weber, O. Faynot, F. Andrieu, C. Buj-Dufournet, F. Allain, P. Scheiblin, J. Foucher, N. Daval, D. Lafond, L. Tosti, L. Brevard, O. Rozeau, C. Fenouillet-Beranger, M. Marin, F. Boeuf, D. Delprat, K. Bourdelle, B.-Y. Nguyen, and S. Deleonibus, "High immunity to threshold voltage variability in undoped ultra-thin FDSOI MOSFETs and its physical understanding," in *IEDM Tech. Dig.*, 2008, pp. 245–248.
- [23] P. R. Kinget, "Device mismatch and tradeoffs in the design of analog circuits," *IEEE J. Solid-State Circuits*, vol. 40, no. 6, pp. 1212–1224, Jun. 2005.
- [24] P. G. Drennan and C. C. McAndrew, "A comprehensive MOSFET mismatch model," in *IEDM Tech. Dig.*, 1999, pp. 167–170.
- [25] F. N. Hooge, "1/f noise source," *IEEE Trans. Electron. Devices*, vol. 41, no. 11, pp. 1926–1935, Nov. 1994.
- [26] P. Su and J. J.-Y. Kuo, "On the enhanced impact ionization in uniaxial strained PMOSFETs," *IEEE Electron. Device Lett.*, vol. 28, no. 7, pp. 649–651, Jul. 2007.
- [27] Y. Taur and T. H. Ning, *Fundamentals of Modern VLSI Devices*. Cambridge, U.K.: Cambridge Univ. Press, 1998, p. 150.



Jack Jyun-Yan Kuo (S'07) was born in Chia-Yi, Taiwan, in 1981. He received the B.S. degree from the Department of Electrophysics, National Chiao Tung University, Hsinchu, Taiwan, and the M.S. degree from the Department of Electrical Engineering, National Chiao Tung University, in 2004 and 2006, respectively. He is currently working toward the Ph.D. degree from the Institute of Electronics, National Chiao Tung University. His current research interests include characterization and modeling of advanced CMOS devices.



William Po-Nien Chen received the B.S. and M.S. degrees in electrical engineering from the National Chiao Tung University, Hsinchu, Taiwan, in 1999 and 2003, respectively.

In 2004, he joined Taiwan Semiconductor Manufacturing Company (TSMC) Ltd., Hsinchu. His current research interests include the physics of semiconductor devices, nanodevice characterizing/modeling, and the carrier-transport mechanism.



Pin Su (S'98–M'02) received the B.S. and M.S. degrees in electronics engineering from the National Chiao Tung University, Hsinchu, Taiwan, and the Ph.D. degree from the Department of Electrical Engineering and Computer Sciences, University of California at Berkeley, Berkeley, in 2002.

From 1997 to 2003, he was a Doctoral and a Postdoctoral Fellow in silicon-on-insulator (SOI) devices at Berkeley. He was also one of the major contributors to the unified BSIMSIOI model, the first industrial standard SOI MOSFET model for circuit design.

Since August 2003, he has been with the Department of Electronics Engineering, National Chiao Tung University, where he is an Associate Professor. His current research interests include silicon-based nanoelectronics, advanced CMOS devices, and device/circuit interactions in ultrascaled CMOS. He has authored or coauthored more than 80 research papers in international journals and conference proceedings.